Table S1 The coefficients of O_3-damaging scheme for a specific PFT.

PFTs	β for high sensitivity (mmol^{-1} m^{-2})	β for low sensitivity (mmol^{-1} m^{-2})	O_3 flux threshold T_{O_3} (mmol m^{-2} s^{-1})
EBF	0.15	0.04	1.6
ENF	0.075	0.02	1.6
DBF	0.15	0.04	1.6
Shrub	0.1	0.03	1.6
Tundra	0.1	0.03	1.6
C_4 grasses	0.735	0.13	5.0
C_3 grasses	1.4	0.25	5.0
C_3 crops	1.4	0.25	5.0
C_4 crops	0.735	0.13	5.0

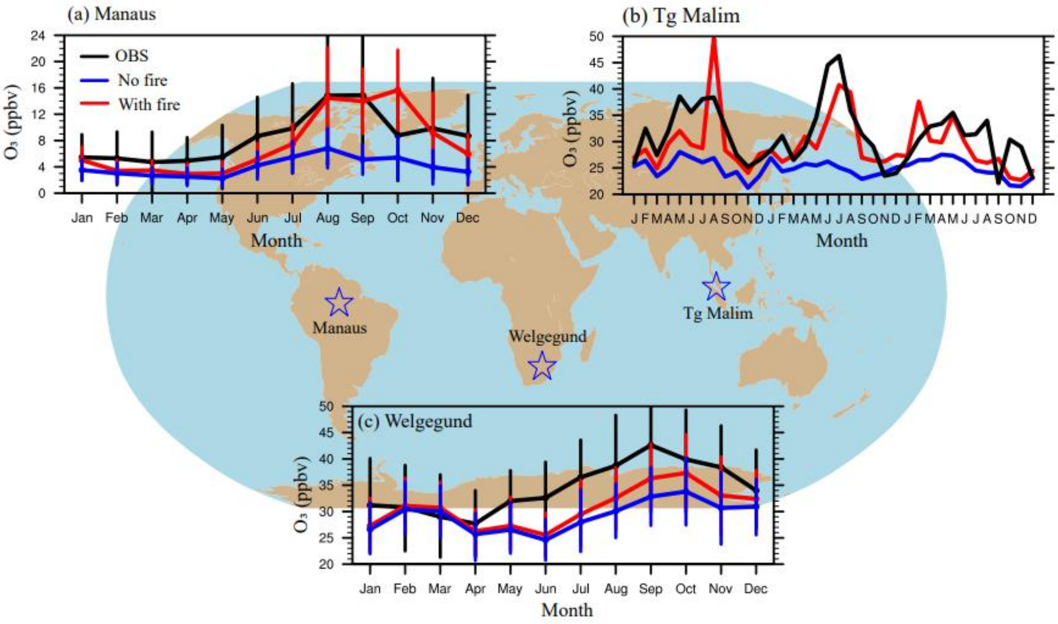

Figure S1 Observed and simulated surface [O_3] at three sites prone to biomass burning: (a) Manaus is from Pope et al. (2020), (b) Tg Malim is from Ahamad et al. (2014), and (c) Welgegund is from Laban et al. (2018). The black lines represent observed [O_3]. The red (blue) lines represent simulated [O_3] with (without) fire emissions. At the Manaus site, the bars represent the values between the 25th and 75th percentiles. At the Welgegund site, the bars represent ±1 standard deviation.

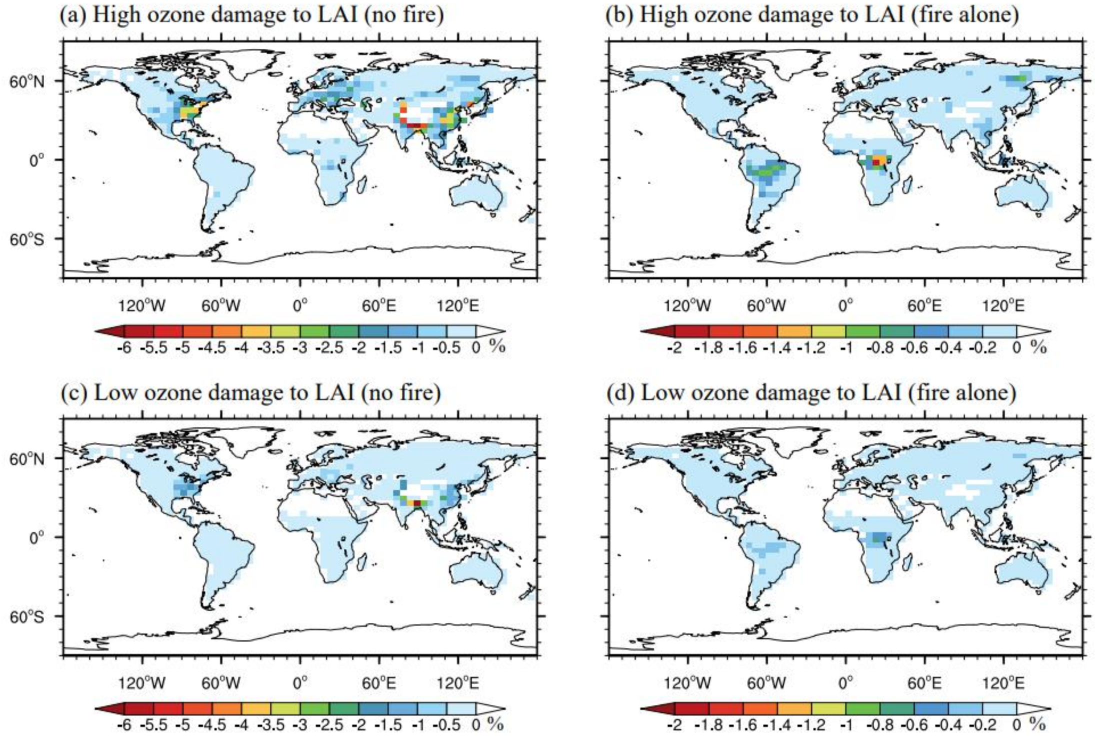

Figure S2 Annual percentage of reductions in leaf area index (LAI) caused by O_3 from (a, c) nonfire and (b, d) fire-alone sources with (a, b) high and (c, d) low O_3 sensitivities. Please note the differences in color scales.

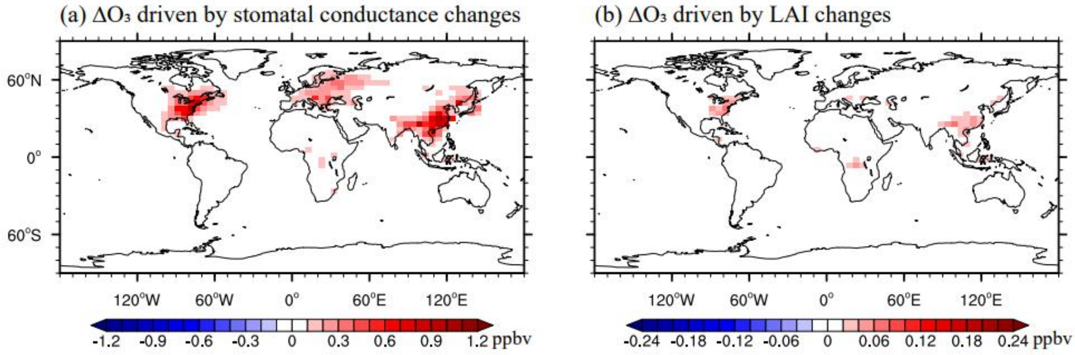

Figure S3 Annual feedback to surface O_3 from nonfire sources with high O_3 sensitivity. **(a)** and **(b)** represent the contributions from stomatal conductance changes and LAI changes, respectively. Please note the differences in color scale.

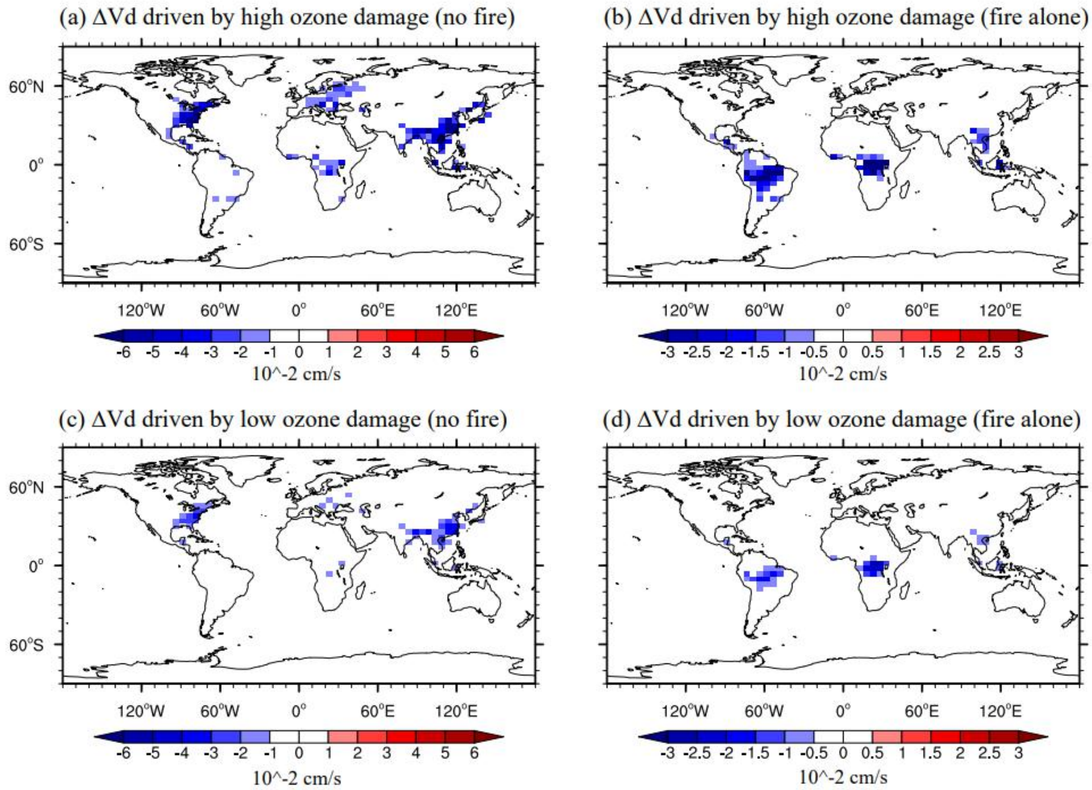

Figure S4 Changes in O_3 dry deposition velocity caused by O_3 vegetation damage with (a, b) high and (c, d) low O_3 sensitivities. (a) and (c) represent damage by O_3 from nonfire sources; (b) and (d) represent damage by O_3 from fire emissions alone. Please note the differences in color scale.

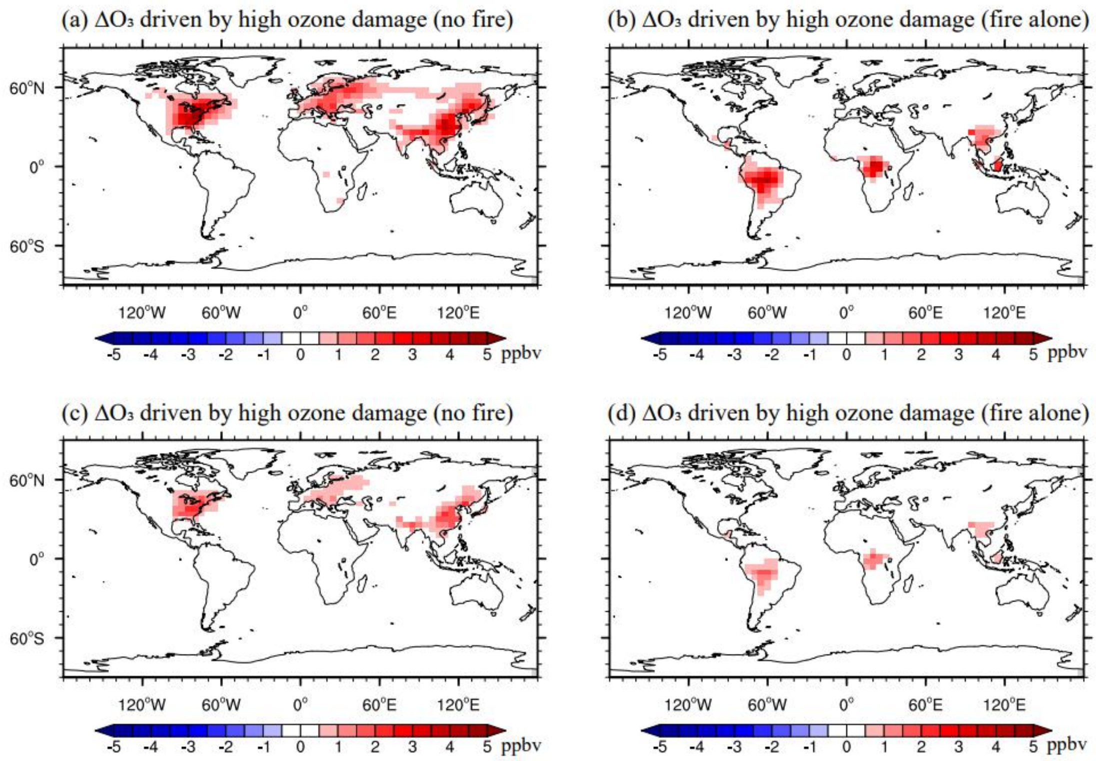

Figure S5 Same as Figure 2 but for extreme O_3-vegetation interactions (average of daily $\Delta[O_3]$ above the 95th percentile).

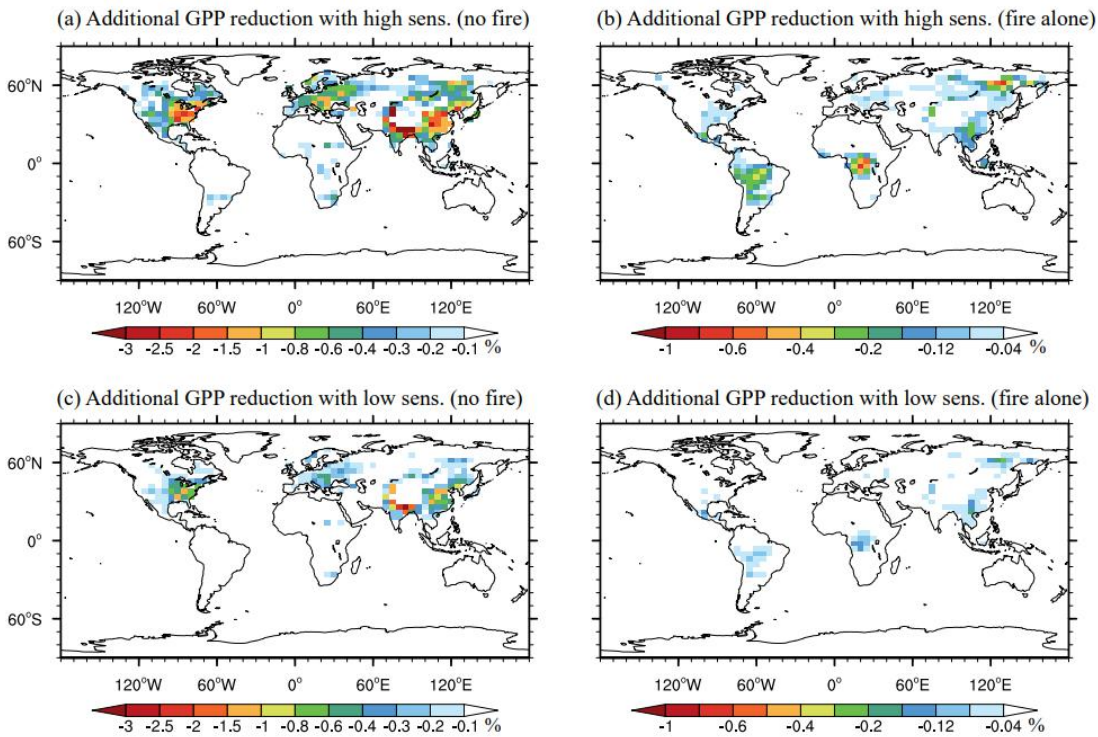

Figure S6 Additional GPP reductions due to increased [O_3] by O_3-vegetation interactions with (a, c) nonfire and (b, d) fire-alone sources. The results are derived as the differences in ΔGPP between the O3OFF and O3CPL simulations (Table 1) using high (a, b) or low (c, d) O_3 sensitivities.

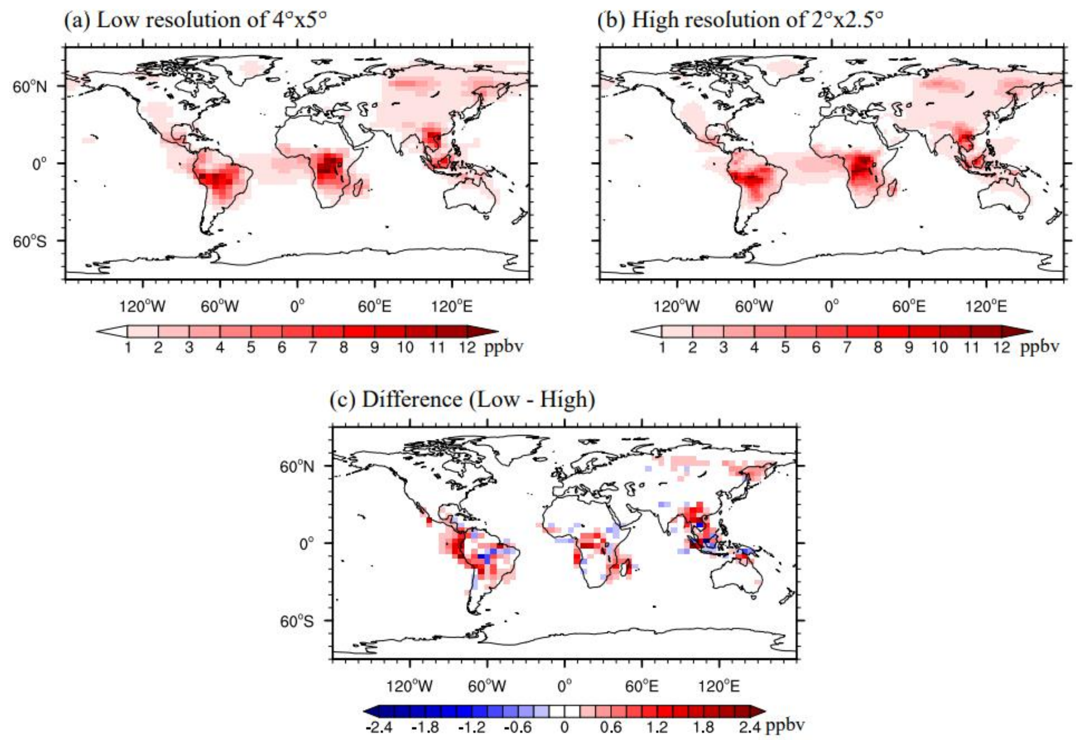

Figure S7 Comparison of the direct contribution of fires to O_3 simulated with (a) low $(4° \times 5°)$ and (b) high $(2° \times 2.5°)$ horizontal resolutions. (c) represents the difference between low and high resolutions (a-b).

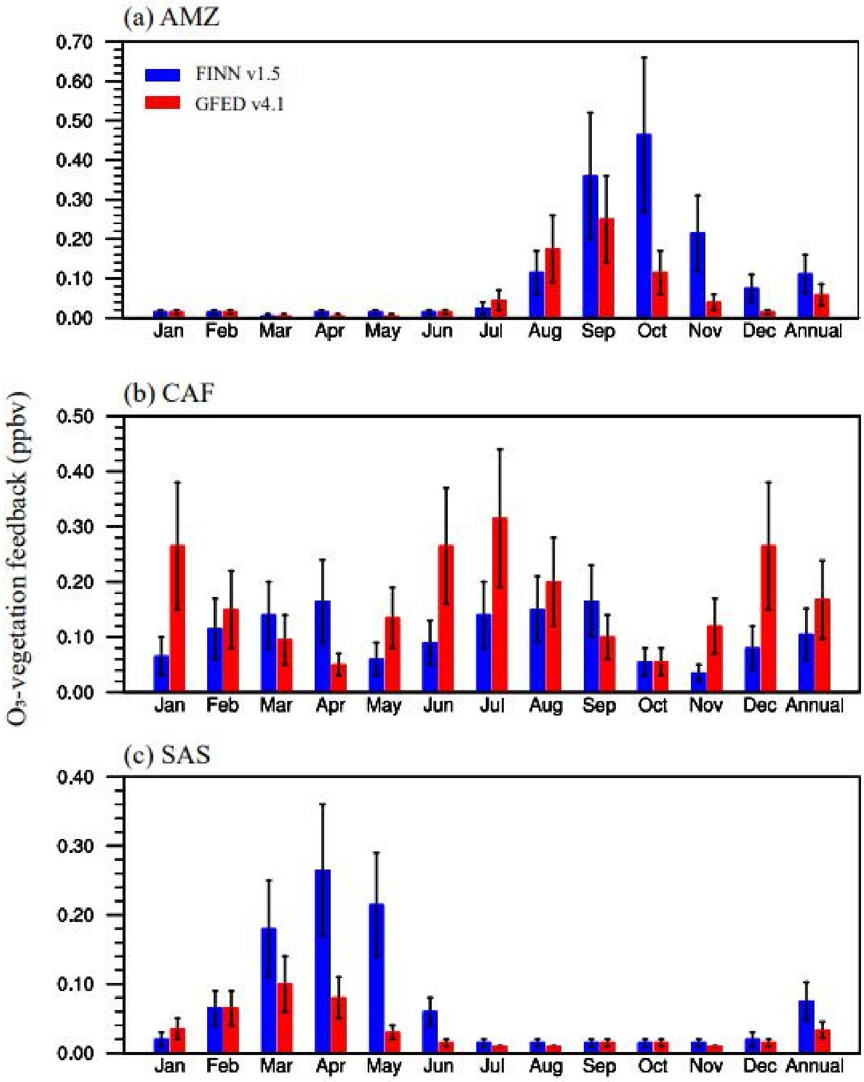

Figure S8 Comparison of O_3-vegetation driven by Fire Inventory from NCAR version 1.5 (FINN v1.5, blue) and Global Fire Emissions Database version 4.1 (GFED v4.1, red) in the Amazon (a), central Africa (b), and southern Asia (c). The error bars represent low to high O_3 damaging sensitivities.

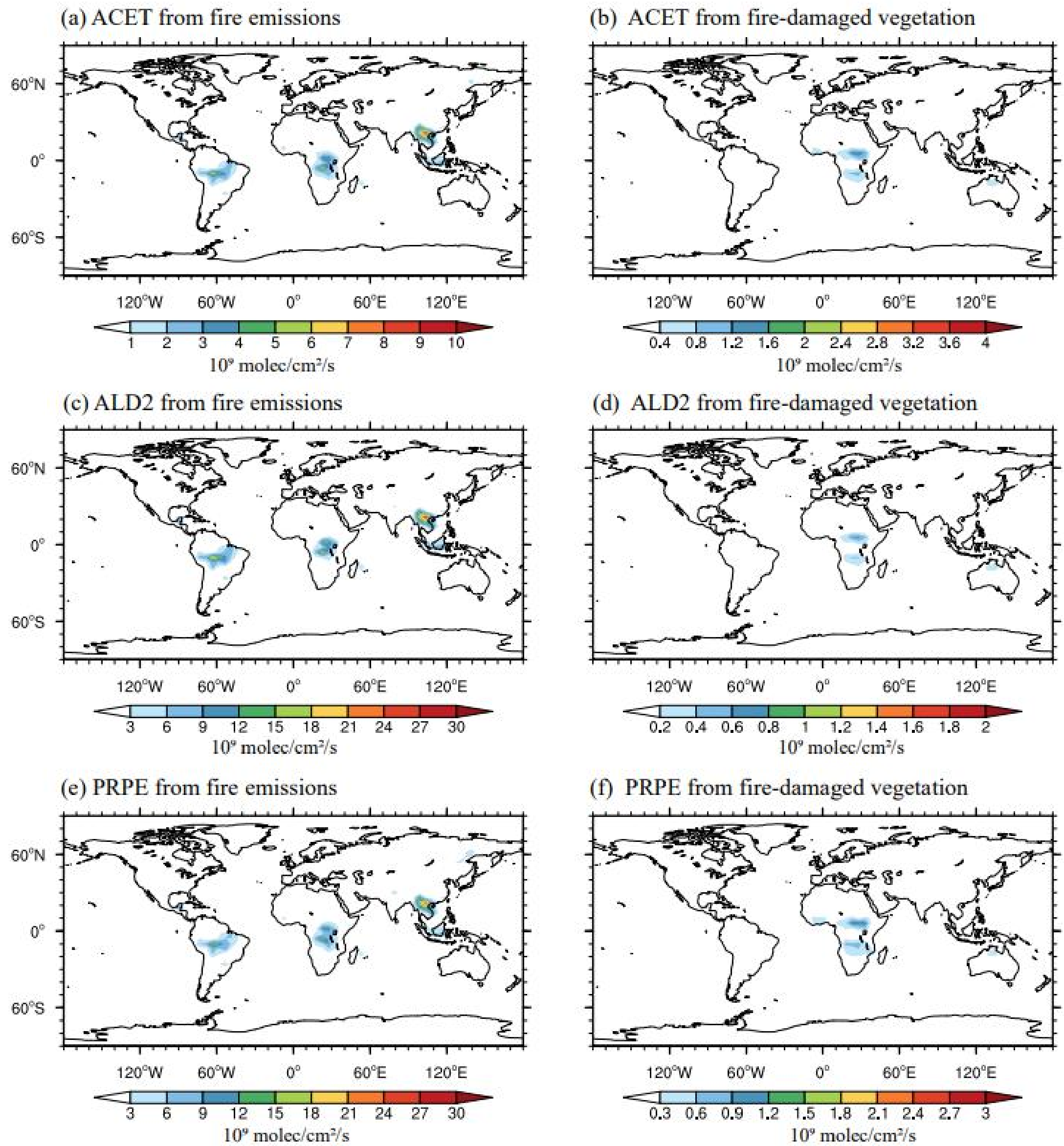

Figure S9 Increased emissions of volatile organic compounds (VOCs) from fire (a, c, e) and reduced VOCs due to fire-induced vegetation loss (b, d, f) in boreal summer. (a) and (b) represent acetone (ACET); (c) and (d) represent acetaldehyde (ALD2); (e) and (f) represent alkenes (PRPE). Please note the differences in color scale.

References

Ahamad, F., Latif, M. T., Tang, R., Juneng, L., Dominick, D., and Juahir, H.: Variation of surface ozone exceedance around Klang Valley, Malaysia, Atmospheric research, 139, 116-127, 2014.

Laban, T. L., Van Zyl, P. G., Beukes, J. P., Vakkari, V., Jaars, K., Borduas-Dedekind, N., Josipovic, M., Thompson, A. M., Kulmala, M., and Laakso, L.: Seasonal influences on surface ozone variability in continental South Africa and implications for air quality, Atmos Chem Phys, 18, 15491-15514, 2018.

Pope, R. J., Arnold, S. R., Chipperfield, M. P., Reddington, C. L., Butt, E. W., Keslake, T. D., Feng, W., Latter, B. G., Kerridge, B. J., and Siddans, R.: Substantial increases in Eastern Amazon and Cerrado biomass burning-sourced tropospheric ozone, Geophys Res Lett, 47, e2019GL084143, 2020.